SUSY SEARCH AND STUDY SCENARIO AT LINEAR e^+e^- COLLIDERS*

KEISUKE FUJII

National Laboratory for High Energy Physics (KEK)
1-1 Oho, Tsukuba, Ibaraki 305, Japan

(Received November 8, 1996)

Experimental aspects of SUSY at future linear e^+e^- colliders are discussed. In particular, the procedures to determine the masses and mixings of SUSY particles are explained with emphasis put on the crucial role of polarized electron beam. These measurements constrain the SUSY breaking parameters and guide us to conduct systematic searches. The implications of the so determined SUSY breaking parameters are discussed also in relation to the GUT scale physics.

PACS numbers: 12.60. Jv, 14.80. Ly

1. Introduction

The existence of at least one light neutral Higgs boson is one of the most important predictions of low energy supersymmetry (SUSY). Its discovery alone is, however, not enough to prove the supersymmetry. It is definitely necessary to find *at least* one supersymmetric particle (sparticle) to show that there is indeed SUSY in nature. Once a sparticle is found, what else can we do then? It is only the beginning and true excitements come after this, which are precision studies of sparticle properties. The existence of a sparticle is a qualitative evidence for the existence of a supersymmetric part ($\mathcal{L}_{\rm SUSY}$) in the Lagrangian of the world ($\mathcal{L}_{\rm world}$). The Lagrangian of the world must contain, however, a supersymmetry breaking (sbreaking) part ($\mathcal{L}_{\rm sbreaking}$), which determines masses and mixings of sparticles. This sbreaking part is believed to be determined by GUT or Planck scale physics and its studies will enable us to make a first realistic step towards the ultra-high energy physics. As illustrated in Fig. 1, experimentalists' tasks can, therefore, be summarized as follows: (1) search for a sparticle to

* Presented at the XXVI Cracow School of Theoretical Physics, Zakopane, Poland, June 1–11, 1996.

qualitatively prove the existence of $\mathcal{L}_{\rm SUSY}$, and (2) determine masses and mixings of sparticles through the measurements of various differential cross sections, thereby testing SUSY quantitatively and uncovering the structure of $\mathcal{L}_{\rm sbreaking}$. In this lecture, I will first demonstrate a typical SUSY scenario

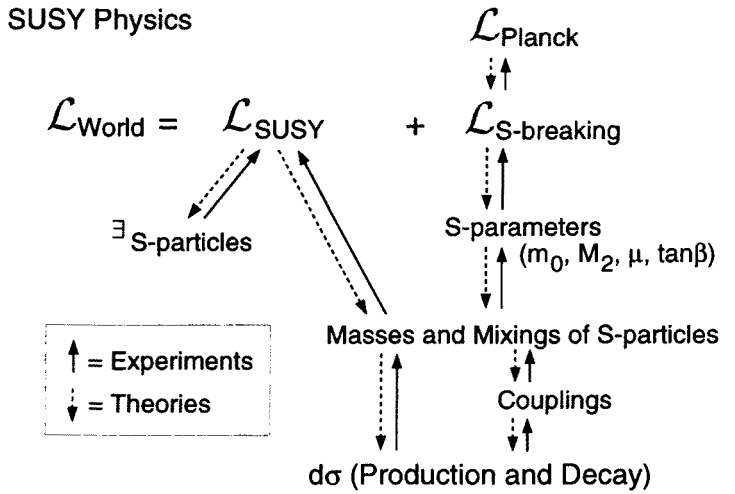

Fig. 1. A schematic diagram showing the relation between the SUSY studies at a future linear e^+e^- collider and GUT or Planck scale physics. The dashed arrows indicate the logical flow of theoretical implications, while the solid arrows show that of experimental inputs.

at a future linear e^+e^- collider, taking a sample case. Third generation slepton (stau) will be treated separately, since it has some very interesting new features. I will then summarize the main points and conclude the lecture.

2. SUSY study scenario; a sample case

Extensive studies have been carried out for SUSY searches at future linear colliders [1]. General conclusion from these studies is that as long as the mass difference between a target sparticle and the lightest SUSY particle (LSP) is not too small, say greater than 20 GeV, its detection at next generation linear e^+e^- colliders is easy. Because of this and time limitation, we are going to skip details of event selection. Instead, we will concentrate on what we can learn from sparticles to be found, taking a sample case.

In order to pick up a typical case, let us first briefly discuss SUSY parameters (sparameters) and their relation to sparticle masses. To be specific, we will work within the framework of supergravity (SUGRA) models with

the "GUT-condition"s, although the search and study methods are largely model-independent and the model assumptions can be tested to a high precision as described later. In these models, the gaugino mass parameters are mutually related through the GUT relation:

$$M_i = M \cdot \frac{\alpha_i(m_Z)}{\alpha_{\rm GUT}}, \tag{1}$$

where $i = 1$, 2, and 3 correspond to $\mathrm{U(1)_Y}$, $\mathrm{SU(2)_L}$, and $\mathrm{SU(3)_C}$, respectively. Reflecting the sizes of the gauge groups, this means, numerically,

$$M_1 : M_2 : M_3 \simeq 1 : 2 : 7 \tag{2}$$

which implies the following inequality between the lighter chargino and the gluino masses:

$$m_{\tilde{\chi}_1^\pm} \lesssim \frac{1}{3} m_{\tilde{g}}. \tag{3}$$

On the other hand, sfermion masses can be written in the form:

$$m_{\tilde{f}}^2 = m_0^2 + G_{\tilde{f}} M^2 + D_{\tilde{f}} m_Z^2, \tag{4}$$

where the first term on the right-hand side is the contribution from the common scalar mass (m_0). The coefficient of the gauge term ($G_{\tilde{f}}$) is controlled by the size of the gauge group to which the sfermion belongs and the coefficient of the D-term ($D_{\tilde{f}}$) depends on $\tan\beta$ and is of O(1) or less. When $M_2^2 \gg m_Z^2$, the sfermion mass spectrum is thus largely determined by the gauge term.

Taking into account the above two mass relations (Eqs (3) and (4)), we can conclude that colored sparticles are heavier than colorless ones and right-handed sfermions are lighter than left-handed ones, in general. Our first SUSY particle (FSP) candidates are thus the lighter chargino ($\tilde{\chi}_1^\pm$) or the right-handed sleptons ($\tilde{l}_{\rm R}^\pm$), except for the light third generation case.

We take a sample parameter set:

$$(m_0, M_2, \mu, \tan\beta) = (70\ \mathrm{GeV}, 250\ \mathrm{GeV}, 400\ \mathrm{GeV}, 2) \tag{5}$$

unless otherwise stated. Using this sample case, I will show you how a typical SUSY scenario goes at the linear collider[2]. This parameter set gives the following sparticle mass spectrum:

$$\begin{aligned}(m_{\tilde{\chi}_1^0}, m_{\tilde{\chi}_2^0}, m_{\tilde{\chi}_1^\pm}, m_{\tilde{l}_{\rm R}}, m_{\tilde{l}_{\rm L}}, m_{\tilde{\nu}_{\rm L}}) \\ = (118, 222, 220, 142, 236, 227)\ \mathrm{GeV}.\end{aligned} \tag{6}$$

Thus our first SUSY particle (FSP) will be the right-handed sleptons pair-produced in e^+e^- collisions.

2.1. Study of $\tilde{l}^{\pm}_{R}(l \neq \tau)$

Since a right-handed slepton decays directly into a lepton plus an LSP, the signal to look for is an acoplanar lepton pair: $e^+e^- \to \tilde{l}^+_R\tilde{l}^-_R \to l^+\tilde{\chi}^0_1 l^-\tilde{\chi}^0_1$. On the other hand, the background to this reaction is standard model (SM) processes with neutrinos which mimic the LSP. The key point here is the power of a highly polarized electron beam available only at linear colliders. For instance, you can eliminate the largest SM background ($e^+e^- \to W^+W^-$ with $W \to l\nu$) very effectively, using a right-handed electron beam: the transverse W-pair production vanishes in the symmetry limit since the s-channel diagram involves a W^0 and the t-channel diagram exchanges a ν_e, both of which only couple to left-handed electrons. On the other hand, the signal cross section will be enhanced because of the weak hypercharge difference between e^-_L and e^-_R: $\sigma_R = 4\sigma_L$ in the symmetry limit. We can see this clearly in Fig. 2, which plots the acoplanarity distributions for smuon pair production with and without the right-handed electron beam. The requirement of $\theta_A > 30°$ eliminates the background to a

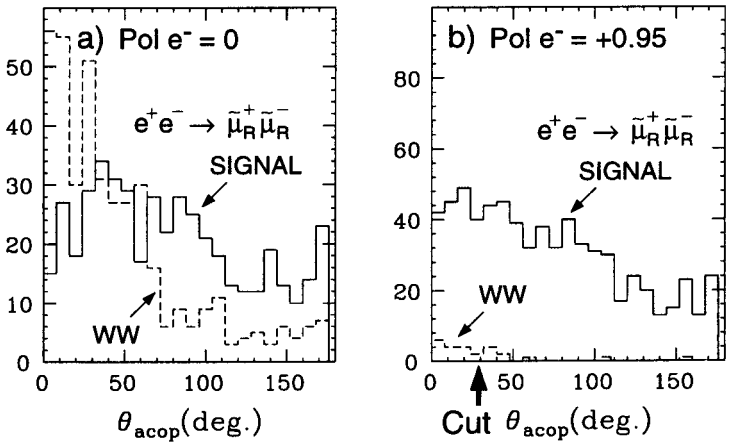

Fig. 2. Examples of acoplanarity distributions for smuon pair productions with (a) an unpolarized beam and (b) a 95 %-right-handed polarized beam. The Monte Carlo data correspond to an integrated luminosity of 20 fb^{-1} at $\sqrt{s} = 350$ GeV. The solid histograms are for the signal events, while the dashed histograms are the background from W^+W^- productions.

negligible level, providing us with a very clean sample for precision studies.

Using this clean sample, we can determine the masses of the LSP and the right-handed slepton through the measurement of the final-state lepton energy distribution (see Fig. 3-a)): the end points of this distribution are

kinematically fixed by the LSP and the slepton masses. A two-parameter fit to this distribution gives a contour plot shown in Fig. 3-b), which tells us that we can determine these masses to a 1% level.

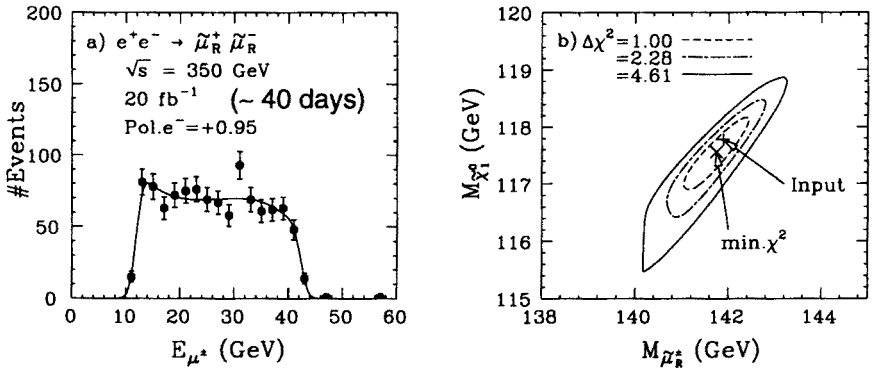

Fig. 3. (a) Energy distribution of muons from smuon decays for the same Monte Carlo parameters as with Fig.2-b). The solid line corresponds to the best fit curve, letting $m_{\tilde{\mu}_R}$ and $m_{\tilde{\chi}_1^0}$ move freely. (b) Contours in the $m_{\tilde{\mu}_R}$-$m_{\tilde{\chi}_1^0}$ plane obtained from the fit to the energy distribution.

With the right-handed selectron and smuon masses determined this way, we can make a very important test of the sbreaking sector, which is a test of generation independence of sfermion masses. The hidden sector SUSY

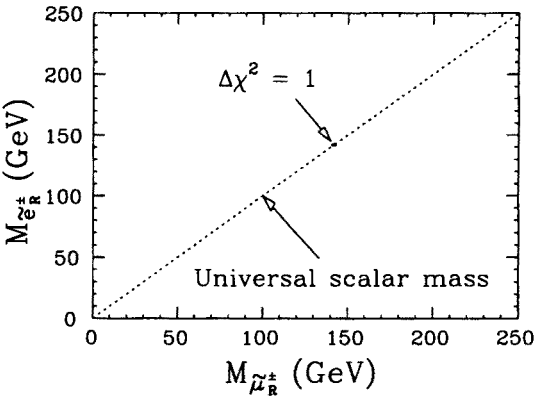

Fig. 4. The expected $\Delta\chi^2 = 1$ contour in the $m_{\tilde{\mu}_R}$-$m_{\tilde{e}_R}$ plane.

breaking implies the universality of scalar masses at the GUT scale, which leads to the mass degeneracy of the first and the second generations. Fig. 4 is an example of the test of the generation independence, demonstrating

potential precision available at the future linear collider.

Now that we know the masses of the LSP and the sleptons, we can solve kinematics up to 2-fold ambiguities. Fig. 5-a) plots the two solutions for the cosine of the smuon production angle. Comparison of this with the corresponding generated one (histogram) suggests that the wrong solution makes a flat background. After the background subtraction, we get the plot in Fig. 5-b), which shows a $\sin^2\theta$ distribution characteristic of s-channel pair productions of a spinless particle. In this way we can confirm that our

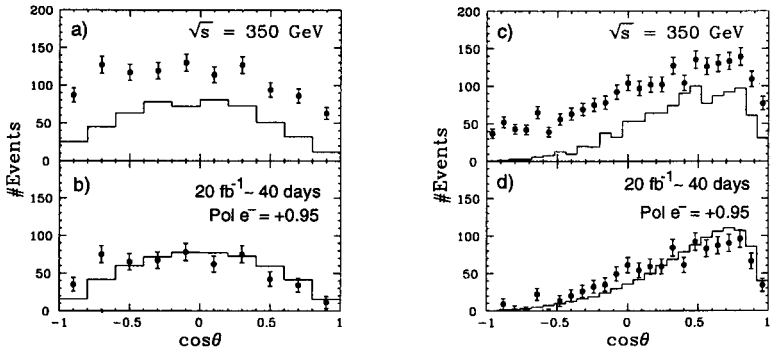

Fig. 5. (a) Production angle distribution of $\tilde{\mu}_R^-$ with respect to the electron beam axis. The points with error bars are the distribution of the two solutions reconstructed from the selected sample corresponding to Fig. 3-a). The histogram is the generated $\cos\theta$ distribution for the selected sample. (b) Production angle distribution after the background subtraction compared with the scaled generated distribution before selection cuts. No acceptance correction is applied to the reconstructed distribution. (c) and (d) are similar plots to (a) and (b) for $e^+e^- \to \tilde{e}_R^+\tilde{e}_R^-$.

smuon is really a scalar particle.

On the other hand, the right-handed selectron pair production has t-channel neutralino-exchange diagrams in addition. Notice that only their bino ($\tilde{B}$) components contribute here, which will produce a forward peak if significant. Figs 5-c) and -d) are similar plots to Figs 5-a) and -b) for the right-handed selectron pair production. The forward peak indicates that our LSP is bino-dominant.

2.2. Study of $\tilde{\chi}_1^\pm$

From the slepton studies, we can determine the mass of the LSP($\tilde{\chi}_1^0$) to better than 1 %. From this we can set an upper limit on the lighter chargino mass, assuming the GUT relation among the gaugino mass parameters. This upper limit corresponds to the gaugino-dominant case ($m_{\tilde{\chi}_1^\pm} \simeq 2 \times m_{\tilde{\chi}_1^0}$),

while the LSP and the lighter chargino will be almost mass-degenerate in the higgsino-dominant case. The upper limit is plotted in Fig. 6 as a function of the LSP mass.

We thus set our center of mass energy just above $4 \times m_{LSP}$ and look for $\tilde{\chi}_1^{\pm}$ pair productions. In our sample case, the chargino decays into a real W and an LSP ($\tilde{\chi}_1^{\pm} \to W^{\pm}\tilde{\chi}_1^0$). The signal to look for will thus be an acoplanar W pair in 4-jet final states. Fig. 7 shows the acoplanarity angle distribution for the signal events (solid histogram) together with major standard-model backgrounds. A cut at $\theta_A = 30°$ will give us a fairly clean sample for precision studies.

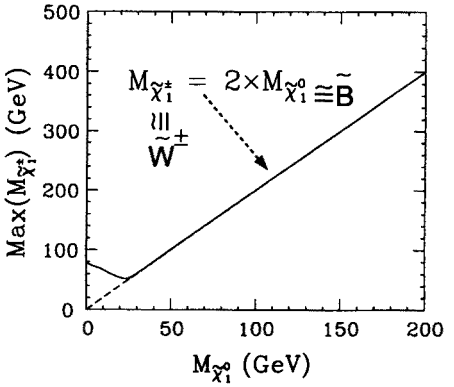

Fig. 6. Upper limit on the lighter chargino mass as a function of the LSP mass, assuming the GUT relation.

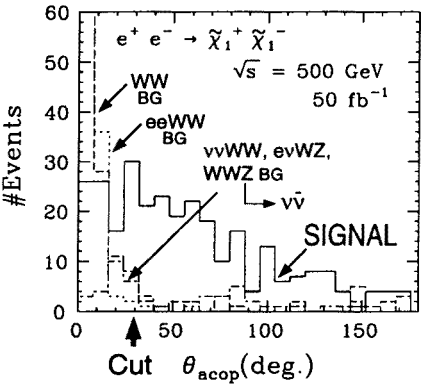

Fig. 7. Acoplanarity angle distribution for $e^+e^- \to \tilde{\chi}_1^+\tilde{\chi}_1^-$ together with major standard-model backgrounds.

As we did to the sleptons, we can first use this clean sample to determine the chargino mass. Fig. 8-a) plots the expected energy distribution of the final-state W's from the chargino decays. The solid curve is the best-fit curve from a 2-parameter fit letting the $m_{\tilde{\chi}_1^{\pm}}$ and $m_{\tilde{\chi}_1^0}$ move freely. Notice that the fit includes the standard-model backgrounds shown as dashed, dot-dashed, and dotted curves, corresponding to those in Fig. 7. Fig. 8-b) is the resultant contour plot in the $m_{\tilde{\chi}_1^{\pm}}$-$m_{\tilde{\chi}_1^0}$ plane, which tells us that we can determine the chargino mass to $\Delta m_{\tilde{\chi}_1^{\pm}} \simeq 8$ GeV. If we use the LSP mass constraint from the slepton study, we can improve this to $\Delta m_{\tilde{\chi}_1^{\pm}} \simeq 5$ GeV.

Using the clean sample, we can also measure the production cross section. Notice that, for the right-handed electron beam, only higgsino components contribute to the chargino pair production in the symmetry limit, since the gauge boson exchanged in the s-channel is B ($U(1)_Y$ gauge boson), which does not couple to wino components. By measuring the production cross section for the right-handed electron beam, we can thus determine the composition of $\tilde{\chi}_1^{\pm}$.

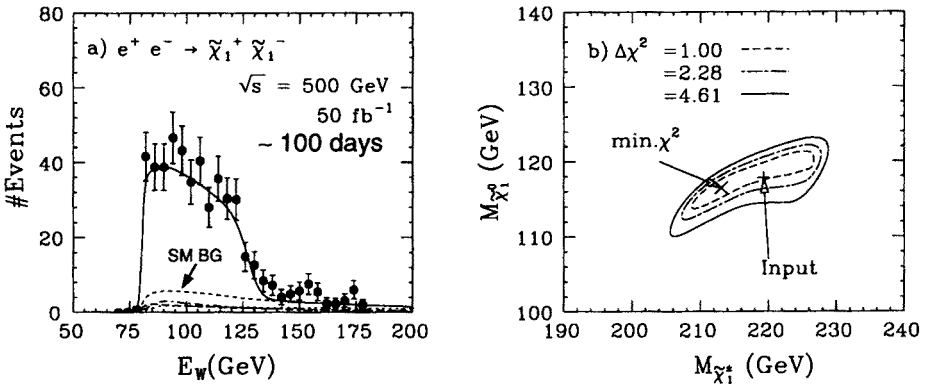

Fig. 8. (a) Energy distribution of final-state W's from chargino decays: $\tilde{\chi}_1^\pm \to W^\pm \tilde{\chi}_1^0$ (points with error bars) for the sample shown in Fig. 7 after the acoplanarity angle cut at $\theta_A = 30°$. The solid curve is the best-fit curve to determine $m_{\tilde{\chi}_1^\pm}$ and $m_{\tilde{\chi}_1^0}$. The other curves correspond to the histograms in Fig. 7. (b) Resultant contours from the 2-parameter fit.

We now know the LSP ($\tilde{\chi}_1^0$) and the chargino ($\tilde{\chi}_1^\pm$) masses, which constrain the chargino and neutralino mass matrices, the production cross section for $e^+e_R^- \to \tilde{e}_R^+\tilde{e}_R^-$, which depends on the bino component of the LSP, and the production cross section for $e^+e_R^- \to \tilde{\chi}_1^+\tilde{\chi}_1^-$, which provides information on the chargino composition. Combining these measurements together, we can carry out a global fit to determine sbreaking parameters: $(M_1, M_2, \mu, \tan\beta)$. Notice that we did not assume the GUT relation between M_1 and M_2 here, since this is what we want to test now. Fig. 9 is the result from such a global fit to Monte Carlo data generated with the GUT relation indicated as a dashed line. In this way, we can test the GUT relation.

The chargino pair production for a left-handed electron beam involves a t-channel exchange of $\tilde{\nu}_e$, which interferes with the s-channel gauge boson exchange diagrams. Since we already know the lighter chargino mass and composition, the only unknown parameter in the cross section is the mass of $\tilde{\nu}_e$. The solid curve in Fig. 10 shows the cross section for the unpolarized electron beam as a function of the mass of $\tilde{\nu}_e$, while the dot-dashed lines indicate the 1-σ bound from the global fit explained above. We can see that the total cross section measurement constrains the sneutrino mass fairly well. Using this and the following model-independent inequality

$$m^2_{\tilde{e}_L^\pm} \leq m^2_{\tilde{\nu}_e} + 0.77 m_Z^2 \,, \tag{7}$$

we can set an upper limit on the left-handed selectron mass. We can thus go and look for the left-handed selectron in $e^+e_R^- \to \tilde{e}_L^+\tilde{e}_R^-$.

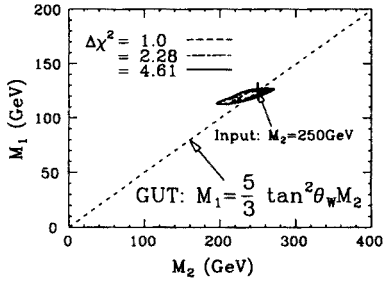

Fig. 9. Constant χ^2 contours in the M_2-M_1 plane obtained from the global fit explained in the text. The dotted line shows the GUT relation.

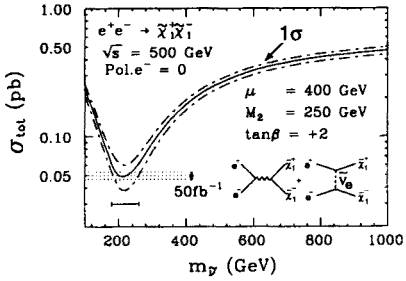

Fig. 10. Lighter chargino pair production cross section as a function of the mass of $\tilde{\nu}_e$. The dot-dashed curves indicate the 1-σ bound from the global fit (see the text).

Before we move on to this, let us try to quantitatively test so far implicitly assumed SUSY[3]. In general SUSY relates mutually supersymmetric couplings: $e_{\rm L}\tilde{W}\tilde{\nu}$ and $e_{\rm L}W\nu$ for instance. This relation can be cast into the form $g = g^\chi$, where g represents the $\mathrm{SU}(2)_{\rm L}$ gauge coupling. For simplicity, let us consider a gaugino-dominant $\tilde{\chi}_1^\pm$ and assume that the chargino mixing is negligible. Then the free parameters that enter the differential cross section for a left-handed electron beam are essentially $m_{\tilde{\nu}}$ and g^χ, since we already know $m_{\tilde{\chi}_1^\pm}$. In order to determine these two unknown parameters, we can use the production cross section ($\sigma_{\rm L}$) and the forward backward asymmetry ($A_{\rm L}^\chi$)[1] for the left-handed electron beam. Fig 11 shows the constraints from the $\sigma_{\rm L}$ and $A_{\rm L}^\chi$ measurements on the two unknown parameters. The horizontal dotted line indicates the SUSY prediction.

If the chargino mixing is significant, the situation will be much better. In such a mixed case, the $\tilde{\chi}_1^\pm$ pair production cross section for the right-handed electron beam is relatively large and measurable with a reasonable precision. The cross section depends on the four parameters contained in the chargino mass matrix:

$$\mathbf{M}_{\tilde{\chi}^\pm} = \begin{pmatrix} M_2 & \sqrt{2}m_W^\chi \sin\beta^\chi \\ \sqrt{2}m_W^\chi \cos\beta^\chi & \mu \end{pmatrix}, \tag{8}$$

where SUSY predicts $m_W^\chi = m_W$. These four parameters can be exchanged for the two masses and two mixing angles: $(m_{\tilde{\chi}_1^\pm}, m_{\tilde{\chi}_2^\pm}, \phi_+, \phi_-)$. Since the mass splitting $(m_{\tilde{\chi}_1^\pm} - m_{\tilde{\chi}_2^\pm})$ is expected to be small and the threshold for

[1] We cannot measure A^χ directly. There is, however, a strong correlation between the asymmetry of $\tilde{\chi}_1^-$ and that of W^-. We can measure the latter using lepton+2-jet final states.

the associate production channel $e^+e^- \to \tilde{\chi}_1^\pm \tilde{\chi}_2^\mp$ is probably not too far away, we can assume that the masses of these two charginos will be fairly well measured, which reduces the number of unknown parameters to two. In order to determine these two unknown phases, we can again use the total pair production cross section (σ_R) and forward-backward asymmetry (A_R^χ) for the right-handed electron beam. The lightly (heavily) shaded region in Fig. 12 is allowed for 30(100) fb^{-1}, which should be compared with the $m_W^\chi = m_W$ contours indicated as dotted lines.

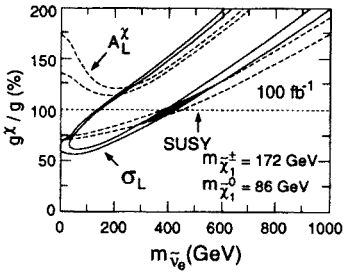

Fig. 11. Constraints in the $m_{\tilde{\nu}}$-g^χ/g plane from σ_L and A_L^χ measurements with 100 fb^{-1} [3] for $(M_2, \mu, m_{\tilde{l}}, m_{\tilde{q}}) =$ (170, −500, 400, 700) GeV and $\tan\beta = 4$.

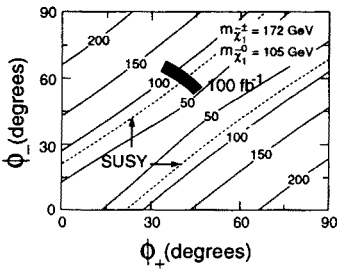

Fig. 12. Constraints in the ϕ_+-ϕ_- plane from σ_R and A_R^χ measurements with 30 (lightly shaded) and 100 fb^{-1} (heavily shaded) [3] for $(M_2, \mu, m_{\tilde{l}}, m_{\tilde{q}}) =$ (210, −195, 400, 700) GeV and $\tan\beta = 4$.

Now that we are convinced with SUSY, we can move on to the left-handed selectron search in $e^+e_R^- \to \tilde{e}_L^+\tilde{e}_R^-$.

2.3. $\tilde{e}_L^\pm$ Study

The associate production of $\tilde{e}_L$ with $\tilde{e}_R$ proceeds via t-channel exchange of neutralinos, to which only the $\tilde{B}$ components contribute. The signal for this process is an acoplanar e^+e^- pair. When we use the right-handed electron beam to suppress standard-model backgrounds, the major background is our previous signal: $e^+e_R^- \to \tilde{e}_R^+\tilde{e}_R^-$. Notice that the use of the right-handed electron beam selects the e^+ in the final state as a carrier of the $\tilde{e}_L$ information. Fig. 13 plots the final-state electron energy against that of the positron, clearly demonstrating this fact. Projecting this to the E_{e^+} axis, we obtain the distribution shown in Fig. 14-a), from which we can extract the sparticle masses as before. The contours from a 2-parameter fit are shown in Fig. 14-b), which tells us that we can determine the left-handed selectron mass to an accuracy better than 1 %.

Knowing both the right-handed and left-handed selectron masses enables us to make another test of the universal scalar mass hypothesis. The

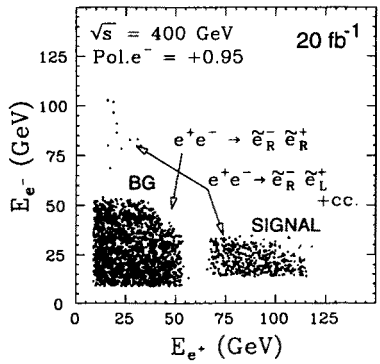

Fig. 13. Distribution of final-state electron energy against that of the positron for $e^+e^-_{\rm R} \to \tilde{e}^+_{\rm L}\tilde{e}^-_{\rm R}$ (signal) and $\tilde{e}^+_{\rm R}\tilde{e}^-_{\rm R}$ (background) at $\sqrt{s} = 400$ GeV with an integrated luminosity of 20 fb^{-1}.

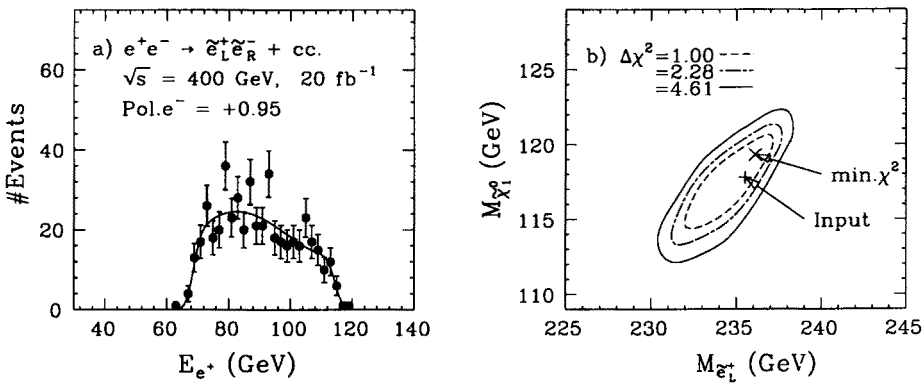

Fig. 14. (a) Energy distribution of positrons from $\tilde{e}^+_{\rm L}$ decays for the same Monte Carlo parameters as with Fig.13. The solid line corresponds to the best fit curve, letting $m_{\tilde{e}_{\rm L}}$ and $m_{\tilde{\chi}^0_1}$ move freely. (b) Contours in the $m_{\tilde{e}_{\rm L}}$-$m_{\tilde{\chi}^0_1}$ plane obtained from the fit to the energy distribution.

squared mass difference of the right-handed (belonging to **5***) and left-handed (belonging to **10**) selectrons is related through the following scalar mass formula:

$$m^2_{\tilde{e}_{\rm L}} - m^2_{\tilde{e}_{\rm R}} = m^2_{0(5)} - m^2_{0(10)} + 0.5M_2^2 - 0.04 \cdot m_Z^2 \cos 2\beta\,. \qquad (9)$$

The universal scalar mass hypothesis implies the representation independence ($m_{0(5)} = m_{0(10)}$), which can be tested as shown in Fig. 15: compare the $\Delta\chi^2 = 1$ contour with the prediction of the universal scalar mass hypothesis (dashed lines for $\tan\beta = 0$ and 30). Notice that the last term

(tan β-dependent term) of the above equation is small and only makes slight difference, allowing us a clean test of the representation independence.

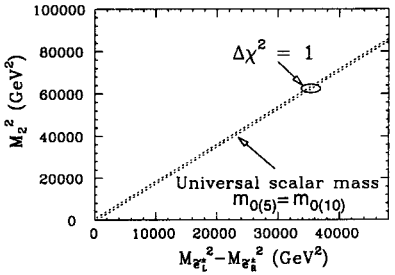

Fig. 15. $\Delta\chi^2 = 1$ contour from the selectron mass measurements, compared with the prediction from the universal scalar mass hypothesis, indicated as dotted lines for $\tan\beta = 0$ and 30.

Once the GUT relation is confirmed and the universal scalar mass hypothesis is verified in the slepton sector, we can set, with confidence, the next target energy for $\tilde{q}$ pair production.

2.4. *Study of* $\tilde{q}_G (G \neq 3)$

A squark may decay into a quark plus an LSP or into a quark plus a chargino or heavier neutralino, depending on the sbreaking parameters. In the former case, the signal for squark pair production is an acoplanar 2-jet final state, while in the latter case it is a final state consisting of two jets plus one or two W/Z bosons from the cascade decays of the charginos or neutralinos, respectively. Potential backgrounds to this process thus include $e^+e^- \to W^+W^-$, $e^{\pm}\overset{(-)}{\nu_e}W^{\mp}$, $\nu\bar{\nu}Z$, $\tilde{\chi}_1^+\tilde{\chi}_1^-$, and $\tilde{\chi}_i^0\tilde{\chi}_j^0$. Notice that the 2-jet systems in the final states of these background processes are all from $W^{(*)}/Z^{(*)}$'s, thereby having invariant masses smaller than 100 GeV. We can therefore very effectively eliminate them by requiring $m_{q\bar{q}} > 100$ GeV, together with usual acoplanar 2-jet selection criteria like $\not{p}_T > 35$ GeV, and $\theta_A > 30°$. We can thus use both e_L^- and e_R^- beams without suffering from these would-be serious backgrounds. It should also be emphasized that the chirality selection of the final-state squarks works better than the slepton case: $\sigma_R(\tilde{q}_R\bar{\tilde{q}}_R) : \sigma_R(\tilde{q}_L\bar{\tilde{q}}_L) \simeq \sigma_L(\tilde{q}_L\bar{\tilde{q}}_L) : \sigma_L(\tilde{q}_R\bar{\tilde{q}}_R) \simeq 9 : 1$, if $m_{\tilde{q}_L} \simeq m_{\tilde{q}_R}$. By controlling the electron beam polarization, we can thus select the chirality of the final-state squarks and, consequently, study their properties separately. Let us first consider the mass determination in the case of the direct decay. In this case, we can use the end-point method as with $\tilde{l}^{\pm}$ and $\tilde{\chi}_1^{\pm}$. There is, however, a better quantity called minimum squark mass ($m_{\tilde{q}}^{\min}$)[4]. defined

by

$$\left(m_{\tilde{q}}^{\min}\right)^2 = E_{\text{beam}}^2 - |\mathbf{p}_1|^2_{\max}$$
$$= E_{\text{beam}}^2 - |\mathbf{p}_2|^2 - |\mathbf{p}_3|^2 + 2|\mathbf{p}_2||\mathbf{p}_3|\cos(\delta+\gamma)\,, \qquad (10)$$

where the momenta and angles are defined in Fig. 16. Notice that the two

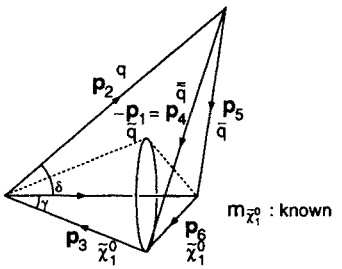

Fig. 16. Definitions of the momenta and angles used to define the minimum squark mass. The LSP mass is assumed to be known precisely.

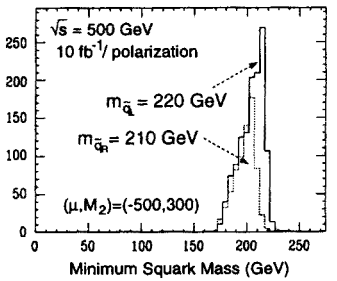

Fig. 17. Expected $m_{\tilde{q}}^{\min}$ distributions for left- and right-handed squarks cited from Ref.[4].

angles δ and γ and the magnitude of the LSP momentum are calculable, provided that the LSP mass is known. Notice also that $m_{\tilde{q}}^{\min}$ makes use of the information contained in the relative configuration of the final-state q and $\bar{q}$ unlike in the end-point method. Fig. 17 shows an example of expected $m_{\tilde{q}}^{\min}$ distributions for parameters shown in the figure. We can see that the Jacobian peaks are good measures of the squark masses and allow their precision measurements: $\Delta m_{\tilde{q}} \simeq 1$ GeV at the 95 % confidence level.

If cascade decays dominate the direct decay, we select final-states with two jets plus leptons and pretent to be blind to the leptons. Notice that these leptons are end-products of the chargino ($\tilde{\chi}_1^{\pm}$) or heavier neutralino ($\tilde{\chi}_2^0$), whose masses are almost degenerate and presumably known from the earlier measurements. We can thus change the role of the LSP in the direct decay case by that of the chargino or second neutralino, by ignoring the final-state leptons. In this way, we can again calculate the minimum squark mass for each event and carry out the squark mass measurement at a 1 % level, provided that $m_{\tilde{\chi}_1^{\pm}}$ and $m_{\tilde{\chi}_1^0}$ are known.

3. Third generation

So far we have been dealing with inos and first and second generation sfermions. Let us now move on to the third generation slepton (stau), which has some very interesting new features.

3.1. $\tilde{\tau}^{\pm}$ Study

As explained below, studies of stau decays provide another handle to uncover the nature of the LSP through the measurement of the final state tau polarization [5]. For simplicity, let us assume that $\tilde{\tau}_L$-$\tilde{\tau}_R$ mixing is negligible and the lighter stau is essentially $\tilde{\tau}_R$. If the LSP is bino-dominant ($\tilde{\chi}_1^0 \simeq \tilde{B}$), the final-state tau will be right-handed ($\tilde{\tau}_R^- \to \tau_R^- \tilde{\chi}_1^0$), since the $\tilde{\tau}\tilde{\chi}_1^0\tau$ coupling stems from the gauge coupling, which is chirality-conserving. On the other hand, if the LSP is higgsino-dominant ($\tilde{\chi}_1^0 \simeq \tilde{H}_1^0$), the $\tilde{\tau}\tilde{\chi}_1^0\tau$ coupling will be of Yukawa type and chirality-flipping, thereby resulting in a left-handed tau in the final state. We can thus determine the nature of the LSP by measuring the final-state tau polarization. Figs 18-a) and -b) shows examples of such a measurement for the bino- and higgsino-dominant cases, respectively. It should be emphasized that this measurement is unique to the stau decays. From the figures, we can see that $\Delta P_\tau \simeq 0.1$ is quite feasible, given an integrated luminosity of 100 fb^{-1}.

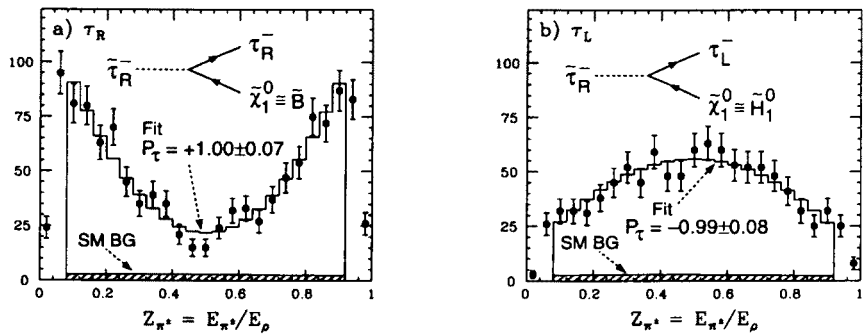

Fig. 18. Distributions of the $\pi^{\pm}$ energy fraction with respect to the energy of the $\rho^{\pm}$ from $\tau \to \nu_\tau \rho$ decays for (a) bino-dominant and (b) higgsino-dominant LSP cases. The points with error bars are the Monte Carlo data corresponding to 100 fb^{-1} with $P_{e^-} = +0.95$ at $\sqrt{s} = 500$ GeV, where $m_{\tilde{\tau}} = 150$ GeV, $m_{\tilde{\chi}_1^0} = 100$ GeV, and $\sigma_{\tilde{\tau}\tilde{\tau}} = 100$ fb are assumed. The shaded histograms are the expected standard-model backgrounds from $e^+e^- \to ZZ, W^+W^-$, $e^+e^-W^+W^-$, and $\nu\bar{\nu}Z$.

As for the mass determinations, we cannot measure the energy distribution of the tau from a stau decay because of a missing neutrino. Nevertheless, we can still measure the energy distribution of the $\rho^{\pm}$ from the tau decay, which carries information on the stau and the LSP masses. Fig. 19-a) plots the reconstructed $E_{\rho^\pm}$ distribution (points with error bars), which is compared with the best fit histogram. The Monte Carlo conditions are the same as with Fig. 18. Fig. 19-b) shows $\Delta\chi^2 = 1$ and 4 contours in the $m_{\tilde{\chi}_1^0}$-$m_{\tilde{\tau}}$ plane, resulting from a two-parameter fit. We can see that, from the $E_{\rho^\pm}$ distribution alone, the stau mass can be determined to an accuracy

of $\Delta m_{\tilde{\tau}}/m_{\tilde{\tau}} = 2\%$ level with an integrated luminosity of 100 fb^{-1}. If we use the $m_{\tilde{\chi}_1^0}$ constraint from the smuon and selectron studies, we can reduce this error on the stau mass to a 1% level.

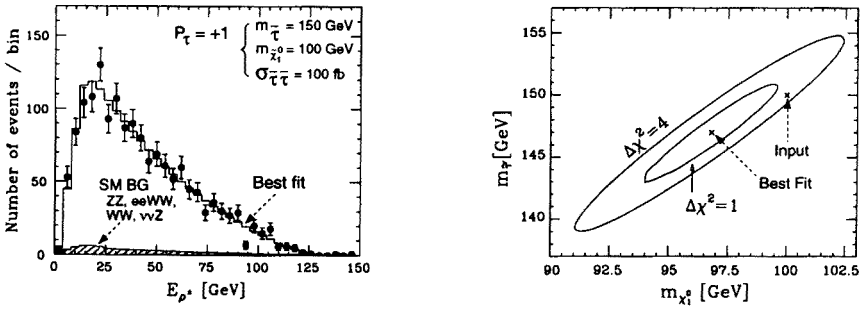

Fig. 19. (a) Energy distribution of $\rho^\pm$'s from $\tau \to \nu_\tau \rho$ decays for the same original Monte Carlo sample as with Fig. 18. The histogram is the best-fit result from a two-parameter fit, letting $m_{\tilde{\chi}_1^0}$ and $m_{\tilde{\tau}}$ move freely. The shaded histograms are the expected standard-model backgrounds from $e^+e^- \to ZZ, W^+W^-$, $e^+e^-W^+W^-$, and $\nu\bar{\nu}Z$. (b) $\Delta\chi^2 = 1$ and 4 contours from the two-parameter fit.

So far we have been ignoring the $\tilde{\tau}_\mathrm{L}$-$\tilde{\tau}_\mathrm{R}$ mixing:

$$\begin{pmatrix} \tilde{\tau}_1 \\ \tilde{\tau}_2 \end{pmatrix} = \begin{pmatrix} \cos\theta_\tau & \sin\theta_\tau \\ -\sin\theta_\tau & \cos\theta_\tau \end{pmatrix} \begin{pmatrix} \tilde{\tau}_\mathrm{L} \\ \tilde{\tau}_\mathrm{R} \end{pmatrix}, \tag{11}$$

through the off-diagonal element of the stau mass matrix:

$$-m_\tau(A_\tau + \mu \tan\beta) \tag{12}$$

which can be sizable, for instance, when μ and $\tan\beta$ are large. The mass ($m_{\tilde{\tau}_1}$) and the pair production cross section ($\sigma_{\tilde{\tau}_1^+\tilde{\tau}_1^-}$) for the lighter stau ($\tilde{\tau}_1^\pm$) are functions of the mixing angle θ_τ. In fact, as can be easily seen from the hyper charge of the mixed state, the cross section for the right-handed electron beam is given, in the symmetry limit, by

$$\sigma_{\tilde{\tau}_1^+\tilde{\tau}_1^-} = \left(\cos^2\theta_\tau + 2\sin^2\theta_\tau\right)^2 \sigma_\mathrm{L}\,, \tag{13}$$

where σ_L here is the cross section when $\tilde{\tau}_1 = \tilde{\tau}_\mathrm{L}$. Fig. 20 shows 1- and 2-σ bounds in the $m_{\tilde{\tau}}$-$\sin\theta_\tau$ plane from the mass and the cross section measurements for an integrated luminosity of 100 fb^{-1} when the pair production cross section is 50 fb. We can see that $\Delta\sin\theta_\tau \simeq \pm 0.05$ is possible, which can be improved to $\Delta\sin\theta_\tau \simeq \pm 0.03$ by including in the $E_\rho^\pm$ fit the $m_{\tilde{\chi}_1^0}$ constraints from the $\tilde{e}_\mathrm{R}$ and $\tilde{\mu}_\mathrm{R}$ studies.

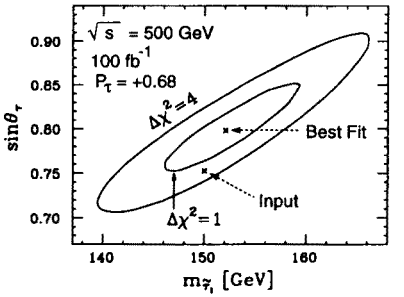

Fig. 20. 1- and 2-σ bounds in the $m_{\tilde{\tau}}$-$\sin\theta_\tau$ plane from the mass and cross section fit for an integrated luminosity of 100 fb^{-1} when the pair production cross section is 50 fb.

3.2. Global fit in the slepton sector

We have seen above that the slepton and the LSP masses can be determined precisely at the linear collider. These mass measurements remove two out of the four free parameters, leaving, for instance, $(M_1, \tan\beta)$ to be fixed by measuring two more observables. As we have seen in the previous section, the total production cross section for $e^+e^-_R \to \tilde{e}^+_R\tilde{e}^-_R$ measures the $\tilde{B}$ content of the LSP ($\tilde{\chi}^0_1$), which is very sensitive to M_1, while being almost independent of $\tan\beta$. On the other hand, the polarization of the τ from a stau decay measures the $\tilde{H}^0_1$ content of the LSP, which depends rather sensitively on $\tan\beta$. The combination of these two measurements thus opens up a possibility to determine $\tan\beta$. Fig. 21 clearly demonstrates these points. In order to see how accurately we can determine $\tan\beta$ with this method, let

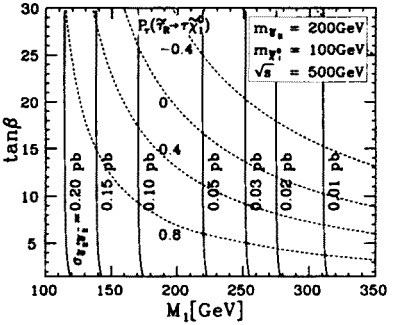

Fig. 21. The total production cross section contours for $e^+e^-_R \to \tilde{e}^+_R\tilde{e}^-_R$ and the polarization contour for the tau from $\tilde{\tau}_R \to \tau\tilde{\chi}^0_1$ in the M_1-$\tan\beta$ plane, when $m_{\tilde{e}_R} = 200$ GeV, $m_{\tilde{\tau}_R} = 150$ GeV, and $m_{\tilde{\chi}^0_1} = 100$ GeV.

us sample typical points in the parameter space and carry out the slepton sector global fit for corresponding Monte Carlo data. Figure 22 summarizes

the results for 100 fb^{-1} at 500 GeV. The input points are sampled along either the $M_1 = 125$ GeV or the $\tan\beta = 15$ lines. The corresponding higgsino mass parameters (μ) are indicated in the figure. We can see that, as the LSP becomes Bino-rich, the sensitivity to $\tan\beta$ quickly goes away. On the other hand, a fairly good $\tan\beta$ measurement is possible if it becomes higgsino-like.

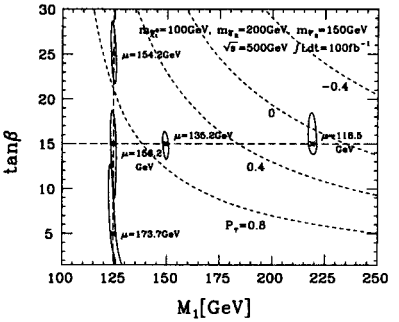

Fig. 22. $\Delta\chi^2 = 1$ contours from the lepton sector global fits described in the text. Five input points are indicated in the figure as crosses.

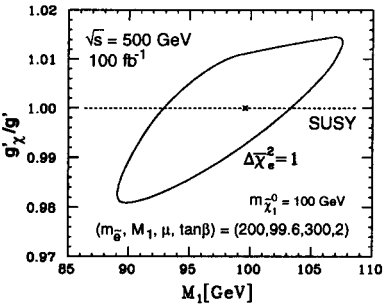

Fig. 23. $\Delta\chi^2 = 1$ contour from the selectron fit described in the text. The dashed line indicates the SUSY relation. The input parameters are $(m_{\tilde{e}_R}, M_1, \mu, \tan\beta)$ = (200 GeV, 99.6 GeV, 300 GeV, 2) corresponding to $m_{\tilde{\chi}_1^0} = 100$ GeV.

We have seen above that, when the LSP is Bino-like, the sensitivity to $\tan\beta$ is at best marginal. We can, however, turn this into an advantage and test SUSY quantitatively. Supersymmetry relates the $e_R\tilde{B}\tilde{e}_R$ coupling ($\sqrt{2}g'_\chi$) to the $\tilde{e}_R B e_R$ coupling (g') as $g'_\chi = g'$. We can test this equality by measuring the differential cross section for $e^+e_R^- \to \tilde{e}_R^+\tilde{e}_R^-$, which is a function of $(m_{\tilde{e}_R}, m_{\tilde{\chi}_1^0}, g'_\chi)$, and the endpoints of the electron energy distribution for the $\tilde{e}_R \to e\tilde{\chi}_1^0$ decays, which determine $m_{\tilde{e}_R}$ and $m_{\tilde{\chi}_1^0}$ model-independently. Figure 23 shows the $\Delta\chi^2 = 1$ contour from the fit to these two observables,

for 100 fb^{-1} at $\sqrt{s} = 500$ GeV. We can see that a percent level test of supersymmetry relation is possible here.

4. Summary and Conclusion

We have quickly gone through a typical SUSY scenario at a future linear e^+e^- collider. Its main features can be summarized as follows. (1) The power of the polarized electron beam will be essential to selecting Feynman diagrams for both signal and background processes, thereby suppressing various backgrounds and sorting out sparticle mixings. (2) The first sparticle alone will provide us with enough information to tell where to go for the next sparticle. (3) We can make precision measurements of various quantities from differential cross sections such as masses, mixing angles, and couplings, which allow us to test SUSY quantitatively and moreover the key assumptions of the supergravity models such as GUT relations, the hidden-sector SUSY-breaking (universal scalar mass), etc. These observations can further be enforced by the studies of the third generation slepton (stau), which have unique features.

We can conclude that the future linear e^+e^- collider will enable us to take a first realistic step towards the GUT/Planck scale physics, once a sparticle is found there.

The author wishes to thank all the members of the JLC working group for useful discussions and comments. In particular, S. Murayama, M. Nojiri, Y. Okada, T. Tsukamoto, M. Yamaguchi deserve special mention, since most of the materials presented here are based on the collaboration with them. The author is very grateful to J. Feng, K. Hikasa, T. Kon, M. Jimbo, M. Peskin, and X. Tata for valuable discussions. Finally the author would like to express his heartfelt gratitude to the workshop organizers, M. Jeżabek in particular, for their efforts to make it so comfortable and so fruitful.

REFERENCES

[1] J. Grivaz, DESY 92-123B p663; R. Becker and C. Vander Velde, DESY 92-123C p457.

[2] T. Tsukamoto, K. Fujii, H. Murayama, M. Yamaguchi, Y. Okada, *Phys. Rev.* **D51**, 3153 (1994).

[3] J. Feng, M. Peskin, H. Murayama, X. Tata, *Phys. Rev.* **D52**, 1418 (1995).

[4] J. Feng, D. Finnell, *Phys. Rev.* **D49**, 2369 (1994).

[5] M. Nojiri, *Phys. Rev.* **D51**, 6281 (1995); M. Nojiri, K. Fujii, T. Tsukamoto, KEK Preprint 96-41, to appear in *Phys. Rev.* **D**.